

Nanoscale

Accepted Manuscript



This is an *Accepted Manuscript*, which has been through the Royal Society of Chemistry peer review process and has been accepted for publication.

Accepted Manuscripts are published online shortly after acceptance, before technical editing, formatting and proof reading. Using this free service, authors can make their results available to the community, in citable form, before we publish the edited article. We will replace this *Accepted Manuscript* with the edited and formatted *Advance Article* as soon as it is available.

You can find more information about *Accepted Manuscripts* in the [Information for Authors](#).

Please note that technical editing may introduce minor changes to the text and/or graphics, which may alter content. The journal's standard [Terms & Conditions](#) and the [Ethical guidelines](#) still apply. In no event shall the Royal Society of Chemistry be held responsible for any errors or omissions in this *Accepted Manuscript* or any consequences arising from the use of any information it contains.

ARTICLE

Mechanical Properties of Amyloid-like Fibrils Defined by Secondary Structures

Cite this: DOI: 10.1039/x0xx00000x

C. Bortolini,^{ab} N. C. Jones,^c S. V. Hoffmann,^c C. Wang,^b F. Besenbacher^a and M. Dong^{*a}Received 00th January 2014,
Accepted 00th January 2014

DOI: 10.1039/x0xx00000x

www.rsc.org/

Amyloid and amyloid-like fibrils represent a generic class of highly ordered nanostructures that are implicated in some of the most fatal neurodegenerative diseases. On the other hand, amyloids, by possessing outstanding mechanical robustness, have also been successfully employed as functional biomaterials. For these reasons, physical and chemical factors driving fibril self-assembly and morphology are extensively studied – among these parameters, the secondary structures and the pH have been revealed to be crucial, since a variation in pH changes the fibril morphology and net chirality during protein aggregation. It is important to quantify the mechanical properties of these fibrils in order to help the design of effective strategies for treating diseases related to the presence of amyloid fibrils. In this work, we show that by changing pH the mechanical properties of amyloid-like fibrils vary as well. In particular, we reveal that these mechanical properties are strongly related to the content of secondary structures. We analysed and estimated the Young's modulus (E) by comparing the persistence length (L_p) – measured from the observation of TEM images by using statistical mechanics arguments – with the mechanical information provided by peak force quantitative nanomechanical property mapping (PF-QNM). The secondary structure content and the chirality are investigated by means of synchrotron radiation circular dichroism (SR-CD). Results arising from this study could be fruitfully used as a protocol to investigate other medical or engineering relevant peptide fibrils.

1. Introduction

Amyloid and amyloid-like fibrils are highly ordered supramolecular nanostructures that are self-assembled from a wide range of polypeptide molecules.¹⁻⁵ In general, amyloid aggregates have become a very important topic to delve into, since they are related to several neurodegenerative diseases such as Alzheimer's and Parkinson's diseases.^{2, 6-11} However, it is worthy to highlight that amyloids, and even the potentially very harmful prion proteins¹²⁻¹⁵, are nowadays successfully employed for technological applications, e.g. memory storage¹⁶ and new multifunctional materials, catalytic scaffolds and bacterial coatings as described by Knowles and co-workers¹⁷. Another aspect promoting the suitability of amyloids is their intrinsic biocompatibility, which means low inflammatory and immunogenic potential.¹⁸

In addition, when compared with metal/carbon nanowires or nanotubes, for which fabrication requirements are very high, self-assembling peptides are more feasibly employed.¹⁹ In particular, non-pathological amyloids, apart from biological functions such as acting as a template for melanin biosynthesis²⁰, have found several applications including drug

delivery, one-dimensional functional nanostructures, nanosensing, as recently reviewed by C. Hauser and co-workers²¹.

Apart from melanin in humans, functional amyloids can be found in animals, such as the silk in moth eggs²², in fungi²³ and in bacteria, such as *curli* in *E. coli*²⁴ that allow bacteria to colonise even steel and as *pili* employed by *Mycobacterium tuberculosis* during human infection.²⁵

All these applications are strongly connected with the structural properties of amyloids. Amyloid fibrils are β -strand rich protein aggregates with different morphologies that constitute a phenomenon known as fibril polymorphism.²⁶⁻²⁹ It has also been demonstrated that fibril morphology directly correlates with cell toxicity.^{3, 30} One of the most important parameters determining these properties is the pH that alters the protein-solvent interactions and the charge of the residues (being zwitterionic amino-acids). These modifications affect self-assembly – different folding events correspond to different secondary and tertiary structure of the final assembled amyloid-based nanostructure. Furthermore, the chirality could be changed by slightly increasing or decreasing the pH around critical values that depend on the particular amyloid compound

under analysis.^{31, 32} In conclusion, the pH plays a crucial role in directing the self-assembly of amyloids from the monomer to the mature stages,^{33, 34} by changing the pH of the environment, different structural topologies of a peptide can be obtained by varying the charge of the peptide and exposed functional groups.

Another important topic is the study of the mechanical properties of amyloid fibrils¹¹ that give important insights about the fibril robustness and open the possibility to know *a priori* the amount of mechanical force necessary to break these structures.³⁵ The relation between pH and secondary structure *versus* nanomechanical properties of amyloid-like peptides has not been investigated yet. The Young's modulus (E), also known as elastic modulus, is a measure of the stiffness of a material.

This work aims to discover the role of the pH and the secondary structures on tuning the Young's modulus of amyloid-like fibrils. For this purpose, the following amino acid sequence has been designed: SSSSFAC – C-terminus is amidated, so serine (S) and cysteine (C) are both N-termini. This short residue sequence is made of a polar region (the 4 serines) located at the N-terminus, and a non-polar region (the two couples of phenylalanine-alanine) and cysteine located at the amidated C-terminus: the peptide is globally amphiphilic, possessing all the requirements to self-assemble into amyloid-like fibrils³⁶.

Atomic force microscopy (AFM) is a very powerful technique to investigate peptide self-assembly³⁷ by following the different aggregation stages and mapping the topography. A complementary technique that provides further structural insights is the transmission electron microscopy (TEM). By analysing a series of EM images and by performing statistical mechanic calculations, the Young's moduli and the persistence length values of different kinds of fibrils can be obtained.^{38, 39}

Instead of using an indirect method, such as the statistical mechanic computation, another possible approach consists of exploiting peak force quantitative nanomechanical property mapping (PF-QNM) to directly obtain an estimation of the Young's modulus.⁴⁰ PF-QNM is an advanced AFM technique that enables quantitative nanomechanical mapping of material properties, including modulus and adhesion, while simultaneously imaging sample topography at high resolution. By analysing AFM images of amyloid-like fibrils obtained with

such a technique, it is possible to estimate the persistence length (L_p) values which can be compared with those obtained by statistical mechanics computation.⁴¹⁻⁴³

Intermolecular forces are known to define material properties of protein nanofibrils.⁴⁴ The different mechanical properties of peptide fibrils may not only be associated with primary and tertiary structures, secondary structure may also play a role. Therefore, in addition to mechanical information about the fibrils, the secondary structure content and the chirality are very important parameters to detect. Circular Dichroism (CD) is a spectroscopic technique able to assess the content of secondary structures in proteins, compute their relative abundance and help identifying the chirality.

2. Results and discussion

The monomer is incubated at room temperature at a concentration of 1 mg/mL. Topographical information about the nanostructures that are forming during incubation are obtained by using AFM (operated as tapping mode). This information, combined with that obtained from negative stained samples from TEM, give a clear overview of all the nanostructures involved in self-assembly. According to the peptide charge chart (see Figure S1 in *Supporting Information*), three pH values (2, 7 and 12) have been chosen as representatives of low, neutral and high pH respectively. AFM and TEM results are in good agreement with each other and show the presence of different kinds of fibrils. All TEM samples are negative stained using a phosphotungstic acid (PTA) 2% solution at pH 7.4.

Figure 1 shows the AFM and TEM images of peptide aggregates. At pH 2 amyloid-like twisted fibrils are forming – a low pH is known to promote fibril formation in amyloids.⁴⁵ The average height value of these fibrils is 3.8 ± 0.2 nm.

At pH 7, similar to samples at pH 2, fibril self-assembly occurs. However, these structures appear more flexible and the twisting characteristic is less pronounced. From the AFM image at pH 7 it is possible to see that fibrils have a strong tendency to bend, even leading to curious "spiral shapes". The average computed height of pH 7 fibrils is 2.2 ± 0.2 nm.

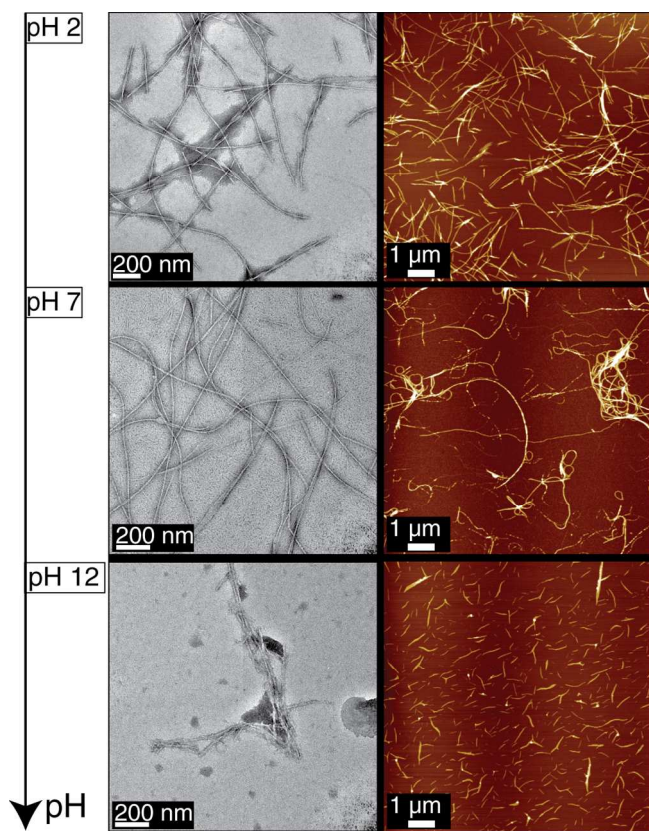


Fig. 1. TEM (left hand side) and AFM (right hand side) images showing the dependence of the peptide from the pH. AFM images are at larger scale bar to provide a broader overview of the structures revealed by TEM.

In order to find an intermediate aggregation state between twisted-pH 2 and flexible-pH 7 fibrils, the peptide has also been incubated at pH 4 – results are shown in Figure S2 in *Supporting Information*. The average computed height of pH 4 fibrils is 3.2 ± 0.2 nm.

The peptide net charge is positive below pH 9 and becomes negative above this value (see Figure S1 in *Supporting Information*). A positive charge – amino acids are more likely to be protonated – favours peptide self-assembly for amyloid-like sequences. Thus, at pH 12 (i.e. negative charge) the monomer aggregates only into peptide fragments which can be identified as bow-like sheet structures³⁶. The average height of pH 12 structures is 2.0 ± 0.1 nm.

Fibrils nanomechanical properties are characterised by exploiting a technique called PF-QNM⁴⁶. Differently from tapping mode AFM, in PF-QNM the vertical motion of the cantilever oscillates far below the resonant frequency using the Z piezo-element and relies on peak force for feedback. Peak interaction force and nanoscale material property information are collected for each individual tap. The resulting force curve plot is then analysed to produce the peak interaction force to give the control feedback signal and the mechanical properties of the sample (e.g. adhesion, modulus, deformation, dissipation). In order to obtain reliable experimental values, it is necessary to perform several calibration procedures. First, the

exact value of the deflection sensitivity is needed; once this has been calculated it is possible to calibrate the spring constant (k) of the AFM tip by thermal tuning. Eventually, the tip radius is assessed. A reference sample is used to measure the deflection sensitivity, for example highly oriented pyrolytic graphite (HOPG), which has a nominal modulus of 18 GPa. As this value is much higher than the expected stiffness value for our samples (i.e. around 2-5 GPa)⁴¹, tip calibration using this substrate is reliable.

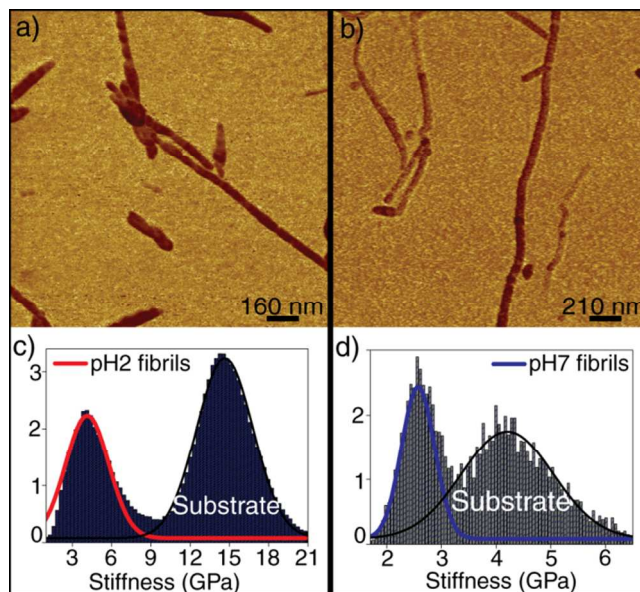


Fig. 2. On top: AFM-PF-QNM images showing the stiffness map of pH 2 (a) and pH 7 fibrils (b). Higher contrast indicates lower stiffness (Young's modulus). On bottom: stiffness value distributions for pH 2 fibrils (c) and pH 7 fibrils (d).

Sapphire is another suitable surface for the nominal stiffness range of the tip (i.e. $k = 20$ to 80 N/m). The loading force was adjusted to give sufficient indentation for reliable measurement of the elasticity, while avoiding damage to the sample. The deformation used was approximately one tenth of the structure height.

Figure 2 shows the stiffness maps of pH 2 (a) and pH 7 fibrils (b). Darker areas correspond to lower Young's modulus values. Figure 2c and 2d present the stiffness values distribution for pH 2 and pH 7 fibrils respectively. Looking at the histograms it is possible to distinguish two main contributions in each image. These are due to the substrate and sample, with the substrate at higher values of stiffness. Fitting the histograms with Gaussian functions the Young's modulus (E) – an average value of the fibrils' stiffness – can be extracted. In such a way, stiffness values for pH 2 and pH 7 fibrils are obtained: $E(\text{pH}2)_{\text{QNM}} = 3.8$ GPa and $E(\text{pH}7)_{\text{QNM}} = 2.5$ GPa. The measured Young's modulus of the background substrate in the pH 7 sample was only 4.5 GPa, significantly lower than expected. Therefore measurements of bare silicon were performed using the same probe for comparison, and a value of 10 GPa was obtained. This indicates the presence of a thin layer of peptide material

on the surface of the substrate for the pH 7 sample, thus reducing the stiffness value recorded for the substrate.

Once E values are obtained, the flexibility of fibrils can be determined and is well expressed by the persistence length (L_p), which is the energy needed in units of $k_B T$ to bend the fibril according to the following equation:⁴⁷

$$L_p = \frac{B}{k_B T} = \frac{EI}{k_B T} \quad (1)$$

where k_b is the Boltzmann constant, B is the bending stiffness (also called flexural rigidity), I is the area momentum of inertia and T is the absolute temperature. Since $k_b T$ is a constant and E is calculated by PF-QNM, the only unknown factor within Equation 1 is the area momentum of inertia, I . I is essentially dependent on the geometry of the object to which the momentum belongs to. By approximating peptide fibrils as cylinders^{41, 48}, the area moment of inertia is: $I = \pi r^4 / 4$, where r is the fibril radius. Usov et al.^{49, 50} described the importance of fibril's shape and polymorphism, showing that the area moment of inertia dramatically depends on the polymorphic form of the amyloids and their real cross section. However, even if pH 2 fibrils appear twisted, AFM images analysis revealed that, in our case, a circular profile is a better approximation than the rectangular one. Therefore, in our work, we adopted a circular cross section both for pH 2 and pH 7 fibrils.

By using the height calculated by the analysis of AFM measurements, fibril radii of $r(\text{pH}2) = 1.9$ nm and $r(\text{pH}7) = 1.1$ nm are found. The corresponding moment of inertia are $I(\text{pH}2) = 10.24$ nm⁴ and $I(\text{pH}7) = 1.15$ nm⁴. Finally, using Equation 1, fibril persistence length values are computed, obtaining $L_p(\text{pH}2)_{\text{QNM}} = 9.47$ μm and $L_p(\text{pH}7)_{\text{QNM}} = 0.70$ μm . As expected, the pH 2 fibrils appear to be much stiffer than those at pH 7, according to AFM calculations (PF-QNM and topography AFM) pH 2 fibrils are roughly 10 times stiffer.

In order to ensure the reliability of these results, a study exploiting statistical mechanics calculation arguments has been carried out. An alternative way to compute the persistence length consists of calculating individual fibril contour lengths (L_c) and end-to-end lengths (R) within the 2D worm-like chain model (2D because fibrils are deposited onto a surface reducing their degrees of freedom), as follows:⁵¹

$$\frac{\langle R^2 \rangle}{L_p^2} = 4L_c L_p \left(1 - \frac{2L_p}{L_c} \left(1 - e^{-\left(\frac{L_c}{2L_p}\right)} \right) \right) \quad (2)$$

A study of more than 150 fibrils for each kind (pH 2 and pH 7) has been performed to obtain a statistically reliable amount of data. Since L_p cannot be analytically computed, ROOT – an object-oriented program and library developed by CERN⁵² – has been employed to fit the data.

Figure 3 shows the results of the computation. At the top of this figure fibril models and TEM micrographs associated with them, are presented. On the bottom, the end-to-end length R is plotted versus the L_c for both pH 2 (Fig. 3a) and pH 7 fibrils

(Fig. 3b). Black dots indicate the pair values for each individual fibril, while the red line is the fit of such data performed by ROOT. The equation used for the fitting is the 2D worm-like chain (Eq. 2). As indicated by the models, pH 2 fibrils appear very stiff having L_c and R very similar, i.e. the fibrils rarely bend. Therefore, it is not a surprise that the standard deviation is very low since a lower amount of “bending events” leads to a more reliable analysis. The persistence length computed for pH 2 is $L_p(\text{pH}2)_{\text{STAT}} = 8.95 \pm 0.69$ μm . This value is slightly lower than that obtained with PF-QNM, however, the difference between these two approaches is only 5.5%. This value is quite lower than the standard error of PF-QNM that can be up to 20%. Thus, statistical mechanics calculations confirm that fibrils from incubation at pH 2 are pretty rigid with Young's modulus values almost 4 GPa.

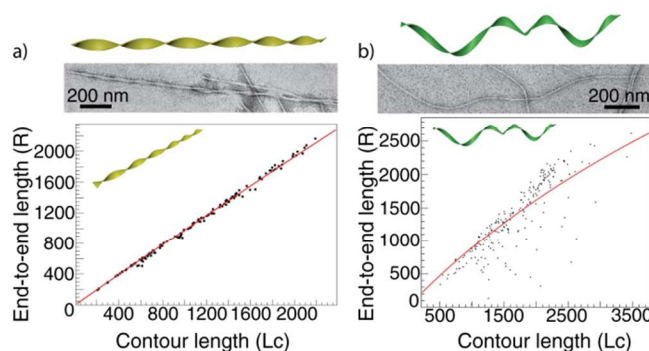


Fig. 3. On top: Fibril model and TEM micrograph of pH 2 (a) and pH 7 fibrils (b). On bottom: Diagrams of the end-to-end length vs the contour length of pH 2 fibrils (a), and pH 7 fibrils (b). Black dots are the computed values, red line is the fit obtained by using the 2D worm-like chain equation (equation 2). Note that the linear end-to-end length (R) is plotted here, as opposed to the square end-to-end length (R^2) on the left-hand side of equation 2, for visual clarity.

Conversely, pH 7 fibrils are very flexible and tend to bend, even forming spirals (see Figure 1, pH 7). The standard deviation is quite large, however, the computed persistence length value is $L_p(\text{pH}7)_{\text{STAT}} = 0.72 \pm 0.16$ μm which is very consistent and almost identical to that calculated using PF-QNM.

	Young's Modulus (E)	Persistence Length (L_p)
pH 2 (QNM)	3.8 GPa	9.47 μm
pH 2 (STAT)	3.6 GPa	8.95 μm
pH 7 (QNM)	2.5 GPa	0.70 μm
pH 7 (STAT)	2.5 GPa	0.72 μm

Table 1. Summary of E and L_p values obtained by PF-QNM and Statistical Mechanics arguments respectively.

Table 1 summarises the values obtained with the QNM and statistical mechanics methods to facilitate the comparison between the E and L_p values. As pH 2 fibrils are more rigid, they exhibit a much higher L_p compared to those at pH 7. However, the Young's moduli are not significantly different as the area moment of inertia for pH 2 is almost 10 times larger than that for pH 7.

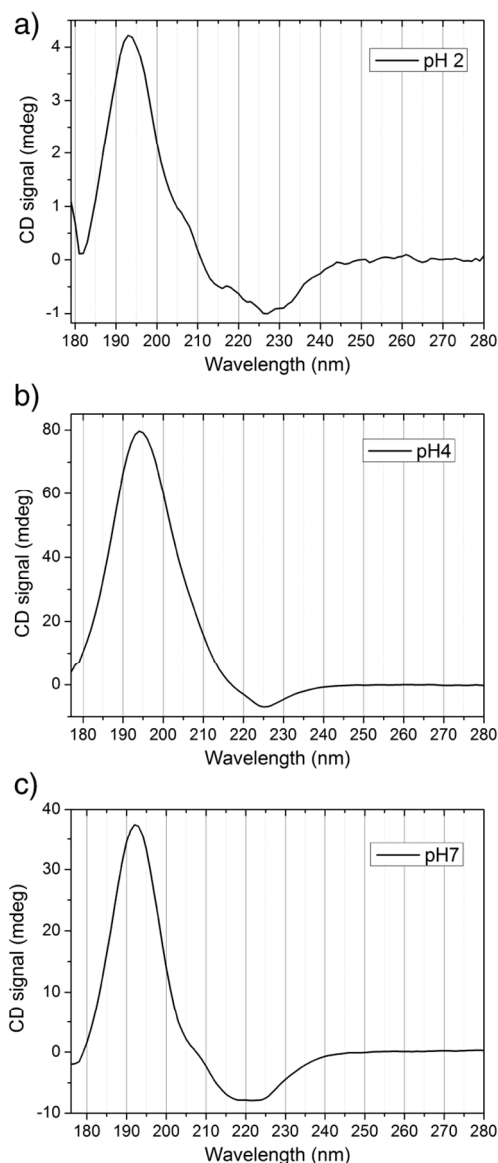


Fig. 4. Synchrotron Radiation Circular Dichroism (SR-CD) spectra of fibrils obtained at pH 2 (a), pH 4 (b) and pH 7 (c), respectively.

So far, we have designed a peptide with a specific primary structure and by changing the pH we obtained different nanostructures which have then been characterised by AFM, PF-QNM and TEM. The difference in the nanomechanical properties have been quantified enabling us to distinguish between stiffer and softer fibrils when observing their tertiary structure. However, it would be interesting to see if there is any correlation between stiffness and secondary structure of the peptides.

It is therefore of interest to investigate the secondary structure content of the fibrils formed by this peptide at the various pHs, to obtain some insight into the nature of the folding and what role they may play in the different mechanical properties exhibited. Figure 4 shows synchrotron radiation circular dichroism (SR-CD) spectra of peptide fibrils from samples

incubated at pH 2 (a), 4 (b) and 7 (c). In addition to the fibrils at pH 2 and pH 7 investigated using AFM and TEM, pH 4 fibrils were also measured (see also Figure S2 in *Supporting Information*) aiming to find an intermediate between the stiffer pH 2 fibrils and the softer pH 7 ones.

In order to perform analyses of SR-CD data shown in Figure 4, we used a web based server called Dichroweb.^{53, 54}

Comparing the CD spectra for all three samples, the overall shape is quite similar, however significantly higher signal is seen for the pH 4 and 7 fibrils indicating a possible higher chirality compared to those at pH 2.

Table S1 (see Supporting Information) illustrates results arising from the analysis of our spectra, differentiating ordered and distorted α -helical and β -sheet structures, turns and random coils. Table S1a shows the relative amount of each structure at the corresponding pH value, while Table S1b, aiming to a more compact view, presents the percentages by distinguishing only α -helices, β -sheets, random coils and turns.

As previously hypothesised, secondary structure content of pH 2 fibrils is quite different from the other kinds of fibrils analysed. Figure 5 summarises the results collected in Table S1 (see Supporting Information).

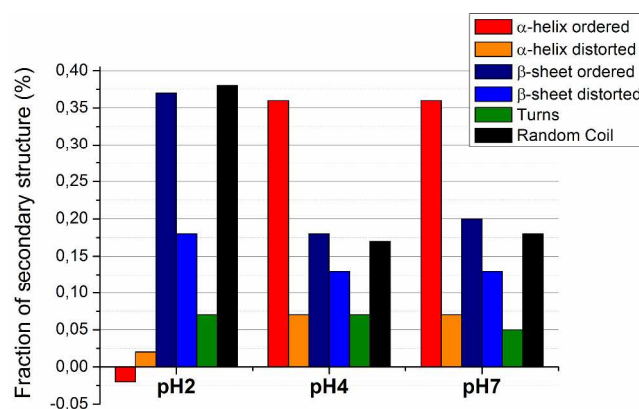


Fig. 5. Histogram showing results from Table 2. While pH 4 and pH 7 look pretty similar, pH 2 fibrils possess a much higher content of ordered β -sheets and random coil and a much lower content of ordered α -helices.

Warm hues indicates α -helices, cool colours β -sheets, green the turns and black for the random coil.

It is known that a high content of β -strands (ordered and unordered mixed up β -domains) contributes to enhance the rigidity of fibrils (e.g. spider silk, β -amyloids)⁵⁵⁻⁵⁷.

Among the three most common kinds of secondary structures – i.e. α -helices, β -strands and random coil – the β -strand is the one possessing the highest number of intermolecular hydrogen bonds. Therefore, nanomechanical properties can, in principle, be affected and improved by the content of β -strands rather than other secondary structures (e.g. fibronectin domains or immunoglobulin domains in titin). In particular, the orientation of β -sheets – regular structures made of β -strands connected laterally by at least a couple of backbone hydrogen bonds – and

the inter-sheet packing are believed to effectively contribute to mechanical properties of peptide fibrils.⁵⁶

As our amyloid-like fibrils formed at pH 2 are stiffer than those at pH 7, we expect a higher content of β -sheets for pH 2 than pH 7 and this is reflected in the results of the secondary structure analysis in Table S1. While the content of turns and distorted structures is similar for all fibrils analysed, random coils and ordered α -helices and β -sheets are very different. In particular, pH 2 fibrils possess a very high amount of ordered β -sheets (37%) and random coil (38%) and no α -helices. Conversely, pH 4 and pH 7 fibrils are very rich in α -helices (43% each) and poorer in ordered β -sheets (18% and 20%) and random coil (17% and 18%). As the spectra for pH 4 and pH 7 are almost identical, it is reasonable to assume that an investigation of nanomechanical properties of pH 4 fibrils by PF-QNM would lead to very similar results to those at pH 7. However, from our experiments it seems that ordered α -helices and β -sheets structures play a crucial role in determining the mechanical properties of peptide fibrils. A high amount of ordered β -sheets contributes to an increase in the rigidity of the fibrils, whereas a high amount of ordered α -helices seems to weaken the structure by softening the self-assembled fibrils. Curiously, the random coils signal – which are structures that cannot be attributed to a specific secondary structure – is a significant part of the stiff pH 2 fibrils, and its content is reduced (like the content of β -sheet) to form α -helices in the softer higher pH value fibrils.

Since CD is a bulk technique, a possibility that cannot be excluded is that some of the α -helices detected with SR-CD at pH 4 and pH 7 are due to the presence of oligomers; therefore, the α -helices signal might be originated not only from the fibrils, but other amyloid aggregates could have contributed to the overall signal. Moreover, several studies have shown that during aggregation proteins acquire a metastable α -helical structure, this was demonstrated for instance for A β 42⁵⁸ and Huntingtin⁵⁹ and it is in general quite probable for an amphiphilic protein.

3. Experimental

3.1 Atomic Force Microscopy (AFM)

AFM experiments were performed in air at room temperature ($21 \pm 1^\circ$, humidity 22%) using a Multimode SPM system with a Nanoscope VIII controller (Veeco Instruments Inc., Santa Barbara, CA). All the recorded AFM images consist of 512 x 512 pixels and several images were obtained at separate locations across the mica surfaces to ensure a high degree of reproducibility of the recorded molecular nanostructures. Samples are prepared by pouring 10 μ l of the peptide solution on a freshly cleaved mica surface, rinsed with distilled water and dried with pressurised air.

3.2 Peak Force Quantitative Nanomechanical Property Mapping (PF-QNM)

Peak force quantitative mechanical measurements were recorded with Peakforce Tapping mode in a commercial Nanoscope VIII MultiMode SPM system (Bruker, Santa Barbara, CA) under ambient conditions. Ultra-sharp silicon tips (Bruker) with a standard spring constant of 20 to 80 N/m and a typical tip radius of 2 nm were used for morphology imaging. The silicon tips – recommended stiffness measurement range 1 GPa < E < 20 GPa (Bruker) – with a spring constant of 200 N/m and a normal tip radius of 8 nm were used for mechanical measurement.

3.3 Transmission Electron Microscopy (TEM)

TEM images were recorded with a Philips C20 transmission electron microscope. To prepare TEM samples, small aliquots of fibril solutions were deposited onto freshly glow-discharged copper grids covered by a thin carbon layer. A droplet of 3 μ l of the fibril solution was deposited on the carbon film for absorption for 1 minute – the excess of fluid was blotted away. Grids were rinsed by applying some droplets of distilled water, followed by blotting. All samples for TEM measurements were negative stained with a solution 1% phosphotungstic acid (PTA) adjusted to pH 7.4.

3.4 Peptides incubation

Monomers were purchased from CASLO Laboratory ApS (Lyngby, Denmark). Monomers were first left to dissolve for one day at room temperature in a hexafluoro-2-propanol (HFIP) concentrated solution (2 mg of peptide in 200 μ l of HFIP solution). Then, the peptide was incubated in an aqueous solution (in which the pH was adjusted by using HCl and NaOH) at room temperature and continually shaken. Final concentration of peptide solution is 1 mg/mL.

3.5 Data Analysis

All the AFM images were analysed by means of the commercial Scanning Probe Image Processor (SPIPTM) software. All force curves were analysed with offline software NanoScope Analysis (Bruker, Santa Barbara, CA).

3.6 Synchrotron Radiation Circular Dichroism (SR-CD)

Synchrotron Radiation Circular Dichroism (SR-CD) spectra were collected on the AU-UV beam line on the ASTRID2 storage ring (ISA, Aarhus University, Denmark). Similar to the CD experiment previously described on the CD1 beam line on ASTRID^{60, 61}, light from the AU-UV beam line was polarized with a MgF₂ Rochon polarizer (B-Halle GmbH, Berlin) and a photo elastic modulator (Hinds, USA) produced alternating left and right handed circular polarized light. The light was then passed through the sample, with concentrations of 1 mg/mL, and was detected by a photo multiplier tube (Type 9406B, ETL, UK). Spectra of water were recorded for baseline subtraction. Samples were measured in a 0.1 mm path-length Suprasil cell (Hellma GmbH). Sample and baseline spectra (1 nm steps size and 2 second dwell time) were each collected in triplicates, averaged and slightly smoothed with a Savitzky-Golay filter using a purpose made Excel template. For Dichroweb, the data

analysis utilised was the CDSSTR programme with reference set SP175 (Optimised for 175-240 nm) and no scaling factor (i.e. the scaling factor is set equal to 1.0).

4. Conclusions

In this work we show that the secondary structure influences the nanomechanical properties of amyloid-like fibrils. AFM and TEM have been employed to follow the fibrillation process and to describe the main features of self-assembled fibrils. By using peak PF-QNM we have measured Young's modulus of peptide fibrils and shown that fibrils formed from the same peptide, but under different pH values, exhibit different morphology and different values of stiffness. Persistence length has been computed by utilising both PF-QNM data and statistical mechanics arguments in order to compare these two methods and obtain reliable values. Moreover, we find that there is a connection between nanomechanical properties of amyloid-like fibrils and its specific secondary structure content: our results indicate that a higher amount of ordered β -sheets contributes to enhance the rigidity while the presence of α -helices appears to soften the nanostructure reducing the Young's modulus. Our results confirm the recent findings reported by Ruggeri et al.⁶² that a higher amount of ordered beta-sheets contributes to enhance the rigidity, while the presence of α -helices appears to soften the nanostructure reducing the Young's modulus.

We believe that these findings are useful to investigate medical related amyloids (such as β -amyloid, α -synuclein and huntingtin protein) and those engineering relevant, offering the possibility of using two reliable methods for the mechanical properties computation and by giving new insights about the role of the secondary structure in regulating the stiffness of peptide fibrils.

Acknowledgements

This work was supported by grants from the Danish National Research Foundation and the Danish Research Agency through support for the iNANO Center and the Danish Council for Strategic Research to iDEA project. M.D. acknowledges a STENO Grant for the Danish Research Council and the VKR Young Investigator Program in Denmark. C.B. acknowledges PhD Scholarship from Sino-Danish Center for Education and Research. In addition, C.B. acknowledges Daniela Saadeh for fruitful discussions about statistical mechanics and the use of ROOT.

Notes and references

^a Interdisciplinary Nanoscience Center (iNANO), Gustav Wieds 14, Building 1590, Aarhus C., Denmark.

^b National Center for Nanoscience and Technology (NCNST), No. 11, Beiyitiao Zhongguancun, Beijing, P. R. China.

^c ISA, Department of Physics and Astronomy, Aarhus University, 8000 Aarhus C., Denmark.

† Footnotes should appear here. These might include comments relevant to but not central to the matter under discussion, limited experimental and spectral data, and crystallographic data.

Electronic Supplementary Information (ESI) available: Supporting Information includes a molecular model for the peptide studied and the charge chart associated to it. In addition, an AFM image of pH 4 fibrils is presented. See DOI: 10.1039/b000000x/

1. C. M. Dobson, *Nature*, 2003, **426**, 884-890.
2. L. C. Walker and M. Jucker, *Nat Neurosci*, 2011, **14**, 669-670.
3. T. Luhrs, C. Ritter, M. Adrian, D. Riek-Loher, B. Bohrmann, H. Doeli, D. Schubert and R. Riek, *P Natl Acad Sci USA*, 2005, **102**, 17342-17347.
4. S. Zhang, S.-J. Cho, K. Busuttill, C. Wang, F. Besenbacher and M. Dong, *Nanoscale*, 2012, **4**, 3105-3110.
5. C. Wang, A. Yang, X. Li, D. Li, M. Zhang, H. Du, C. Li, Y. Guo, X. Mao, M. Dong, F. Besenbacher, Y. Yang and C. Wang, *Nanoscale*, 2012, **4**, 1895-1909.
6. E. D. Roberson and L. Mucke, *Science*, 2006, **314**, 781-784.
7. D. M. Holtzman, J. C. Morris and A. M. Goate, *Sci Transl Med*, 2011, **3**.
8. D. L. Brody, S. Magnoni, K. E. Schweteye, M. L. Spinner, T. J. Esparza, N. Stocchetti, G. J. Zipfel and D. M. Holtzman, *Science*, 2008, **321**, 1221-1224.
9. D. J. Selkoe, *Nature*, 2003, **426**, 900-904.
10. F. Chiti and C. M. Dobson, *Annu Rev Biochem*, 2006, **75**, 333-366.
11. T. P. J. Knowles and M. J. Buehler, *Nat Nanotechnol*, 2011, **6**, 469-479.
12. G. Miller, *Science*, 2009, **326**, 1337-1339.
13. P. Brundin, R. Melki and R. Kopito, *Nat Rev Mol Cell Bio*, 2010, **11**, 301-307.
14. B. Frost and M. I. Diamond, *Nat Rev Neurosci*, 2010, **11**, 155-159.
15. G. Lamour, C. K. Yip, H. B. Li and J. Gsponer, *Acs Nano*, 2014, **8**, 3851-3861.
16. J. Shorter and S. Lindquist, *Nat Rev Genet*, 2005, **6**, 435-450.
17. T. P. J. Knowles, T. W. Oppenheim, A. K. Buell, D. Y. Chirgadze and M. E. Welland, *Nat Nanotechnol*, 2010, **5**, 204-207.
18. I. Macindoe, A. H. Kwan, Q. Ren, V. K. Morris, W. R. Yang, J. P. Mackay and M. Sunde, *P Natl Acad Sci USA*, 2012, **109**, E804-E811.
19. X. H. Yan, P. L. Zhu and J. B. Li, *Chem Soc Rev*, 2010, **39**, 1877-1890.
20. L. Rochin, I. Hurbain, L. Serneels, C. Fort, B. Watt, P. Leblanc, M. S. Marks, B. De Strooper, G. Raposo and G. van Niel, *P Natl Acad Sci USA*, 2013, **110**, 10658-10663.
21. C. A. E. Hauser, S. Maurer-Stroh and I. C. Martins, *Chem Soc Rev*, 2014.
22. V. A. Iconomidou, G. Vriend and S. J. Hamodrakas, *Febs Lett*, 2000, **479**, 141-145.
23. S. Dos Reis, B. Coulary-Salin, V. Forge, I. Lascu, J. Begueret and S. J. Saupe, *J Biol Chem*, 2002, **277**, 5703-5706.
24. M. R. Chapman, L. S. Robinson, J. S. Pinkner, R. Roth, J. Heuser, M. Hammar, S. Normark and S. J. Hultgren, *Science*, 2002, **295**, 851-855.

25. C. J. Alteri, J. Xicohtencatl-Cortes, S. Hess, G. Caballero-Olín, J. A. Girón and R. L. Friedman, *P Natl Acad Sci USA*, 2007, **104**, 5145-5150.
26. A. T. Petkova, R. D. Leapman, Z. H. Guo, W. M. Yau, M. P. Mattson and R. Tycko, *Science*, 2005, **307**, 262-265.
27. J. D. Pham, B. Demeler and J. S. Nowick, *J Am Chem Soc*, 2014, **136**, 5432-5442.
28. L. R. Volpatti, M. Vendruscolo, C. M. Dobson and T. P. J. Knowles, *Acs Nano*, 2013, **7**, 10443-10448.
29. C. Bortolini, L. Liu, Z. Li, K. Thomsen, C. Wang, F. Besenbacher and M. Dong, *Advanced Materials Interfaces*, 2014, n/a-n/a.
30. M. Anderson, O. V. Bocharova, N. Makarava, L. Breydo, V. V. Salnikov and I. V. Baskakov, *J Mol Biol*, 2006, **358**, 580-596.
31. D. Kurouski, R. K. Dukor, X. F. Lu, L. A. Nafie and I. K. Lednev, *Chem Commun*, 2012, **48**, 2837-2839.
32. D. Kurouski, R. K. Dukor, X. F. Lu, L. A. Nafie and I. K. Lednev, *Biophys J*, 2012, **103**, 522-531.
33. Y. Arii and K. Hatori, *Biochem Biophys Res Commun*, 2008, **371**, 772-776.
34. W. Hoyer, T. Antony, D. Cherny, G. Heim, T. M. Jovin and V. Subramaniam, *J Mol Biol*, 2002, **322**, 383-393.
35. J. F. Smith, T. P. J. Knowles, C. M. Dobson, C. E. MacPhee and M. E. Welland, *P Natl Acad Sci USA*, 2006, **103**, 15806-15811.
36. C. Bortolini, L. Liu, T. M. A. Gronewold, C. Wang, F. Besenbacher and M. Dong, *Soft Matter*, 2014, **10**, 5656-5661.
37. L. Liu, K. Busuttill, S. Zhang, Y. L. Yang, C. Wang, F. Besenbacher and M. D. Dong, *Phys Chem Chem Phys*, 2011, **13**, 17435-17444.
38. C. Lara, I. Usov, J. Adamcik and R. Mezzenga, *Phys Rev Lett*, 2011, **107**.
39. C. Lara, J. Adamcik, S. Jordens and R. Mezzenga, *Biomacromolecules*, 2011, **12**, 1868-1875.
40. S. Zhang, M. Andreassen, J. T. Nielsen, L. Liu, E. H. Nielsen, J. Song, G. Ji, F. Sun, T. Skrydstrup, F. Besenbacher, N. C. Nielsen, D. E. Otzen and M. D. Dong, *P Natl Acad Sci USA*, 2013, **110**, 2798-2803.
41. J. Adamcik, A. Berquand and R. Mezzenga, *Appl Phys Lett*, 2011, **98**.
42. J. Adamcik and R. Mezzenga, *Curr Opin Colloid In*, 2012, **17**, 369-376.
43. J. Adamcik, J. M. Jung, J. Flakowski, P. De Los Rios, G. Dietler and R. Mezzenga, *Nat Nanotechnol*, 2010, **5**, 423-428.
44. T. P. Knowles, A. W. Fitzpatrick, S. Meehan, H. R. Mott, M. Vendruscolo, C. M. Dobson and M. E. Welland, *Science*, 2007, **318**, 1900-1903.
45. R. Srinivasan, E. M. Jones, K. Liu, J. Ghiso, R. E. Marchant and M. G. Zagorski, *J Mol Biol*, 2003, **333**, 1003-1023.
46. J. Adamcik, C. Lara, I. Usov, J. S. Jeong, F. S. Ruggeri, G. Dietler, H. A. Lashuel, I. W. Hamley and R. Mezzenga, *Nanoscale*, 2012, **4**, 4426-4429.
47. G. S. Manning, *Phys Rev A*, 1986, **34**, 4467-4468.
48. K. K. M. Sweers, M. L. Bennink and V. Subramaniam, *J Phys-Condens Mat*, 2012, **24**.
49. I. Usov, J. Adamcik and R. Mezzenga, *Acs Nano*, 2013, **7**, 10465-10474.
50. S. Jordens, E. E. Riley, I. Usov, L. Isa, P. D. Olmsted and R. Mezzenga, *Acs Nano*, 2014, **8**, 11071-11079.
51. S. Jordens, L. Isa, I. Usov and R. Mezzenga, *Nat Commun*, 2013, **4**.
52. R. Brun and F. Rademakers, *Nucl Instrum Meth A*, 1997, **389**, 81-86.
53. L. Whitmore and B. A. Wallace, *Nucleic Acids Res*, 2004, **32**, W668-W673.
54. L. Whitmore and B. A. Wallace, *Biopolymers*, 2008, **89**, 392-400.
55. A. Nova, S. Ketten, N. M. Pugno, A. Redaelli and M. J. Buehler, *Nano Lett*, 2010, **10**, 2626-2634.
56. S. B. Xiao, S. J. Xiao and F. Grater, *Phys Chem Chem Phys*, 2013, **15**, 8765-8771.
57. E. T. Pashuck, H. G. Cui and S. I. Stupp, *J Am Chem Soc*, 2010, **132**, 6041-6046.
58. M. D. Kirkitadze, M. M. Condrón and D. B. Teplow, *J Mol Biol*, 2001, **312**, 1103-1119.
59. R. Mishra, M. Jayaraman, B. P. Roland, E. Landrum, T. Fullam, R. Kodali, A. K. Thakur, I. Arduini and R. Wetzel, *J Mol Biol*, 2012, **415**, 900-917.
60. A. J. Miles, S. V. Hoffmann, Y. Tao, R. W. Janes and B. A. Wallace, *Spectrosc-Int J*, 2007, **21**, 245-255.
61. A. J. Miles, R. W. Janes, A. Brown, D. T. Clarke, J. C. Sutherland, Y. Tao, B. A. Wallace and S. V. Hoffmann, *J Synchrotron Radiat*, 2008, **15**, 420-422.
62. F. S. Ruggeri, J. Adamcik, J. S. Jeong, H. A. Lashuel, R. Mezzenga and G. Dietler, *Angewandte Chemie International Edition*, 2015, **54**, 2462-2466.